All-optical nonlinear Breit-Wheeler pair production with γ-flash photons

Alexander J. MacLeod [1,*] Prokopis Hadjisolomou [1] Tae Moon Jeong [1] and Sergei V. Bulanov [1,2]

[1]*ELI Beamlines, International Laser Research Centre, Institute of Physics, Czech Academy of Sciences, Za Radnicì 835, 25241 Dolnì Břežany, Czech Republic*

[2]*National Institutes for Quantum and Radiological Science and Technology, Kansai Photon Science Institute, 8-1-7 Umemidai, Kizugawa, Kyoto 619-0215, Japan*

(Received 27 October 2022; accepted 13 December 2022; published 20 January 2023)

High-power laser facilities give experimental access to fundamental strong-field quantum electrodynamics processes. A key effect to be explored is the nonlinear Breit-Wheeler process: the conversion of high-energy photons into electron-positron pairs through the interaction with a strong electromagnetic field. A major challenge to observing nonlinear Breit-Wheeler pair production experimentally is first having a suitable source of high-energy photons. In this paper we outline a simple all-optical setup which efficiently generates photons through the so-called γ-flash mechanism by irradiating a solid target with a high-power laser. We consider the collision of these photons with a secondary laser and systematically discuss the prospects for exploring the nonlinear Breit-Wheeler process at current and next-generation high-power laser facilities.

DOI: 10.1103/PhysRevA.107.012215

I. INTRODUCTION

Modern advances in laser technology have brought us into the multipetawatt laser power regime, with a large number of high-power laser facilities [1] either operational or in development (see, e.g., [2–14]). High-power lasers generate intense electromagnetic fields, allowing access to the nonlinear regime of quantum electrodynamics (QED), where the interaction between particles and laser fields cannot be described by the usual methods of vacuum perturbation theory. Instead, the electromagnetic field must be taken into account nonperturbatively through a framework typically referred to as strong-field QED [15–19]. One of the most important strong-field QED phenomena is the nonlinear Breit-Wheeler (NBW) process [20–23]: The production of an electron-positron pair from the interaction between a high-energy γ-photon and strong electromagnetic field. High-power lasers are an ideal source of strong fields, with field strengths $E_0 \sim 10^{-3}E_S$ already achieved experimentally with petawatt-class systems [4], where $E_S \sim 1.32\times10^{18}$ V m^{-1} is the Schwinger critical field of QED at which nonperturbative pair production occurs [24–26].

With high-power lasers supplying the strong fields, one still requires a source of γ photons for NBW experiments. The source should ideally meet the following criteria.

(i) High energy. The NBW process is exponentially suppressed when the quantum nonlinearity parameter for a photon with momentum l_μ, $\chi_\gamma = \sqrt{-(F_{\mu\nu}l^\nu)^2}/mcE_S \ll 1$, becoming more probable as $\chi_\gamma \gtrsim 1$. If the field strength of the laser pulse is parametrized by the dimensionless intensity parameter $\xi = eE_0\lambda_C/\hbar\omega_0$,[1] this corresponds to a photon energy $\omega_\gamma \gtrsim m^2/2\omega_0\xi$. Typical multipetawatt laser facilities will operate with optical frequencies $\omega_0 \sim 1$ eV and field strengths $\xi \sim 10^2$–10^3, requiring photons with energy in the MeV to GeV range.

(ii) Large numbers. The total number of generated electron-positron pairs $\mathcal{N}_{e^-e^+}$ is directly proportional to the number of photons which collide with the laser $\mathcal{N}_{e^-e^+} \propto \mathcal{N}_\gamma$.

(iii) Synchronized. Multipetawatt laser systems reach high peak power by compressing laser pulses to femtosecond durations. The photon source should be easily synchronized with the colliding pulse to ensure that large numbers of photons pass through the spatiotemporal region of highest field strength.

(iv) Overlap. High intensities are achieved by focusing laser pulses to (typically) micron beam waists w_0. The photon beam should have large spatial overlap with the laser focal spot to mitigate the impact of shot-to-shot fluctuations.

(v) Efficient. The photon-generation mechanism should efficiently convert the total input energy into a comparable total energy of photons.

Different photon sources suitable for strong-field QED experiments have been proposed, which generally fall into two categories: electron seeded or laser driven (for a review see, e.g., [27] and references therein).

Electron-seeded schemes generate γ photons by colliding electron bunches with electromagnetic fields or high-Z targets. In the former case, photons can be produced in the perturbative regime $\xi \ll 1$ via inverse Thomson or Compton scattering [28]. or in the nonperturbative regime $\xi \gtrsim 1$ via

*alexander.macleod@eli-beams.eu

[1]Here e is the electron charge, E_0 is the electric-field strength, $\lambda_c = \hbar/mc$ is the Compton wavelength of an electron with mass m, and ω_0 is the central frequency of the laser pulse.

nonlinear Compton scattering [22,29,30]. The weak-field case $\xi \ll 1$ produces radiation which is highly monochromatic and polarized [31–33], but requires high-density electron bunches of GeV energy to produce the significant numbers of MeV photons [31,34] required for the NBW process. In the nonlinear regime $\xi \gtrsim 1$, electron bunches of comparatively lower density can be used to generate high-brightness photon beams with energy comparable to the initial energy of the electrons (see, e.g., [35,36]), due to the high field strengths causing significant portions of the electron energy to be radiated. Alternatively, electron beams can be collided with high-Z targets to produce photons via bremsstrahlung [37,38], where the maximum photon energy is again comparable to the initial electron energy. This scheme has shown promise for the study of the NBW process [39] and is being considered as the primary source of photons in several experimental proposals (see, e.g., [40–43]). Novel schemes have also been proposed utilizing electron-beam–multifoil collisions [44] and high-density electron bunch collisions with solid targets [45] to produce γ photons with high conversion efficiency.

The key limiting factor of each of these approaches is the initial step of producing high-energy, high-density electron beams. This must be achieved using conventional RF accelerators or laser-wakefield acceleration (LWFA) [46–48]. Conventionally-accelerated electron beams were utilized in the first experimental demonstration of pair production in the weak-field regime ($\xi \ll 1$) [49,50] and will be used in the upcoming LUXE campaign to explore pair production in the transition regime ($\xi \gtrsim 1$) [40]. However, currently no facility exists which hosts *both* a conventional accelerator and a multipetawatt laser system, putting the nonperturbative multiphoton regime of the NBW process ($\xi \gg 1$) out of reach with this approach. Therefore, LWFA will be the primary mechanism for producing electron bunches at multipetawatt laser facilities. A typical photon source using LWFA electrons will require multiple stages. First, the electrons are produced through a single or multistage acceleration scheme with an initial laser pulse colliding with an underdense plasma. Second, depending on the properties of the electron beam such as its transverse size and divergence, these will need to be focused or columnated to achieve higher densities and mitigate undesirable features in the produced photons (see, e.g., [39]). Finally, the electrons will generate photons via one of the mechanisms outlined above, requiring either another laser pulse or strong-field source, or collision with a high-Z target. At each stage in the photon-generation scheme, nonlinear plasma effects, shot-to-shot fluctuations in laser parameters and/or electron-beam properties, and the spatiotemporal size of the produced photon beams can make synchronization with another colliding laser pulse extremely challenging. Furthermore, the conversion efficiency between the initial laser energy and the total energy of the produced photons can be extremely low.

Instead of using electrons to generate γ photons, one can instead hope to produce them more directly using a laser-driven approach. While many of the electron-seeded schemes described above would require multistage experimental configurations and access to high-energy electron sources such as conventional accelerators, laser-driven γ-photon generation can typically be achieved in a single stage, with the only requirement being access to a high-power laser. A simple scheme which uses high-power lasers to irradiate solid targets is the so-called γ-flash mechanism [51,52]. The γ-flash mechanism meets all of the desired properties (i)–(v) outlined above, producing large numbers of MeV to GeV photons with very high conversion efficiency between the laser energy and the energy of the produced photons [53–68]. Furthermore, the use of only a single laser-driven stage to generate the γ flash, coupled with the short duration and large transverse size of the photon beam, makes synchronization to and overlap with a secondary laser pulse particularly simple.

In this paper we investigate the feasibility of using the γ-flash mechanism for studying nonlinear Breit-Wheeler pair production through an extremely simple all-optical two-stage configuration, demonstrated in Fig. 1. The key physical parameter which limits the attainable on-target peak power at a high-power laser facility is the total available pulse energy E_{total}. Our scheme assumes E_{total} is split between two laser pulses $E_{\text{total}} = E_{\text{flash}} + E_{\text{pairs}}$. A pulse of energy E_{flash} is used to irradiate an overdense plasma, chosen as solid Li, to drive γ-photon production through the γ-flash mechanism. This produces a γ-photon beam with large numbers of MeV to GeV photons, which propagate out from the rear surface of the target. A second laser pulse, with energy E_{pairs}, collides head-on with the γ photons at an interaction distance d from the target rear surface to produce electron-positron pairs through the NBW process.

The paper is structured as follows. In Sec. II we discuss the angular and spectral properties of photons generated through the γ-flash mechanism. The spectra are produced using the particle-in-cell (PIC) code EPOCH [76]. In Sec. III we summarize theoretical aspects of the NBW process, giving expressions for the differential probability of pair production from the collision of a photon and a linearly polarized plane-wave pulse with a Gaussian temporal envelope. In Sec. IV numerical results are presented for the total number of electron-positron pairs produced through the interaction of γ-flash photons with high-power laser pulses. We consider three different cases of total available laser pulse energy E_{total}, relevant for current- and next-generation laser facilities, and discuss the optimal partitioning of this energy into E_{flash} and E_{pairs} to maximize the overall pair yield. We also discuss the energy and angular properties of the produced positrons. In Sec. V we summarize our key findings and discuss future steps for refining and optimizing our approach. Throughout the rest of the paper we work in natural units $\hbar = c = 1$ unless otherwise specified and use the shorthand notation $a^\mu b_\mu \equiv a \cdot b$ and $b \cdot b \equiv b^2$ with metric tensor $g_{\mu\nu} = \text{diag}(+1, -1, -1, -1)$.

II. THE γ-FLASH PHOTON SPECTRUM

At low intensities, overdense plasmas, where the electron density $n_e > n_{\text{cr}}$, with $n_{\text{cr}} = \epsilon_0 m_e \omega_0^2 / e^2$ the critical density for frequency ω_0, are opaque to laser light. Irradiating an overdense plasma with a laser of sufficiently high intensity induces relativistic transparency, allowing the laser to propagate into the plasma and drive electron motion. A dense QED plasma is produced where there is an interplay between field-induced QED phenomena and collective plasma effects [51,52].

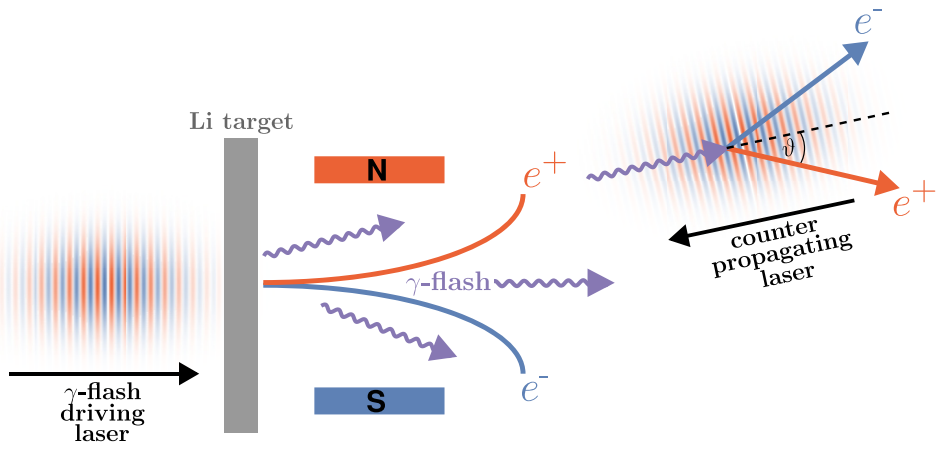

FIG. 1. Proposed experimental configuration. The total available laser energy E_{total} is split into two beams: $E_{\text{total}} = E_{\text{flash}} + E_{\text{pairs}}$. The beam with energy E_{flash} is used to irradiate a solid lithium target, producing high-energy photons via the so-called γ-flash mechanism [51,52]. Charged secondary particles from the target are deflected to minimize background. The γ-flash photons propagate from the rear surface of the lithium target and collide with a counterpropagating secondary pulse, energy E_{pairs}, to produce electron-positron pairs via the nonlinear Breit-Wheeler mechanism [20–23]. Positrons are emitted at an angle ϑ relative to the axis of the colliding counterpropagating laser.

Copious numbers of high-energy photons are generated by charged particles in the QED plasma by a combination of nonlinear Compton scattering [51,52] and bremsstrahlung [37,38], in a mechanism often referred to as a γ-flash. Numerical studies primarily utilizing PIC codes [51,52] have demonstrated that the laser-to-photon energy conversion efficiency κ_γ for the γ-flash mechanism can be as large as several tens of percent for single laser [53–61], dual laser [62–64], and multilaser configurations [65–68].

The first stage of our setup involves irradiating an overdense plasma with an intense laser pulse to generate high-energy photons. The plasma is taken to be a solid Li target, of density $n_e \approx 1.39\times10^{29}$ m^{-3}, with a diameter of 12 μm and a thickness of 10 μm. The choice of target is twofold. First, thin low-Z targets are known to reduce secondary particle production by photons in the material, compared to thicker and/or higher-Z targets (see, e.g., [69–71]). Second, Li has previously been shown to optimize the laser-to-photon energy conversion efficiency with metallic targets [61]. To increase the efficiency of photon generation the target is first irradiated with a long prepulse which generates a conical channel and has an effect similar to using targets fabricated with cone structures (see, e.g., [61,71–74]). The three-dimensional electron number density for the structured target is reproduced from a publicly available data set [75] which calculates the effect of the prepulse using radiation hydrodynamic simulations. These data are then used as the initial conditions for the three-dimensional PIC simulations which model photon generation using the code EPOCH [76] compiled with the Higuera-Cary [77], bremsstrahlung, and photon [78] directives enabled.

We consider the γ-photon spectra generated from lasers with different values of the laser energy E_{flash}. In each case the pulse is a linearly polarized laser with a full width at half maximum (FWHM) duration of 17 fs focused at normal incidence on the target with beam waist $w_0 \sim 1.86$ μm. The central laser wavelength is $\lambda_0 = 0.815$ μm, typical of Ti:sapphire laser systems [79] used at many current- and next-generation facilities (see, e.g., [3,4,7,9–11]). These parameters are summarized in Table I.

Photons are emitted in a symmetric double-lobe pattern due to the transverse motion of electrons in the plasma (see, e.g., [52,60,61,80–82]). The angular distribution of the radiant intensity of the γ-flash photons from the rear surface of the Li target for three different laser energies $E_{\text{flash}} = (85, 255, 850)$ J is shown in Fig. 2. For the constant parameters in Table I, these correspond to laser powers $P_{\text{flash}} = (5, 15, 50)$ PW and approximate intensities $I_{\text{flash}} \sim (5\times10^{22})$–$(5\times10^{23})$ W cm^{-2} (or equivalently $\xi_{\text{flash}} \sim$ 150–475). An angle of $\theta = 0^\circ$ corresponds to emission along the laser-beam axis. The radiant intensity of the γ-flash photons has been averaged over the symmetric double-lobe emission pattern.

By colliding the produced photons with a secondary laser pulse, they will act as seed photons for the NBW process. This process requires a large flux of high-energy photons and so to maximize the number of pairs produced the secondary laser should be focused to the region of highest radiant intensity. The energy spectra which will be used in the calculation of the NBW process in Sec. IV will correspond to the γ-flash photons within the full-angle divergence of $\beta = 10^\circ$ which maximizes the radiant intensity. The appropriate region for each of the different laser powers is shown as the shaded portions of Fig. 2. These are found to be centered around $\theta = (32^\circ, 22^\circ, 23^\circ)$ for $P_{\text{flash}} = (5, 15, 50)$ PW, respectively.

The differential energy spectra $\omega_\gamma d\mathcal{N}_\gamma(\omega_\gamma)/d\omega_\gamma$ [energy ω_γ and differential number of photons $d\mathcal{N}_\gamma(\omega_\gamma)/d\omega_\gamma$] of the γ-flash photons are shown in Fig. 3. Dark solid curves give the full angular spectra, with the light dashed curves showing the spectra corresponding photons within the $\beta = 10^\circ$ full-angle divergence shaded regions of Fig. 2. The photons

TABLE I. Constant laser parameters for the γ-flash driving laser with energy E_{flash}.

τ_{FWHM} (fs)	λ_0 (μm)	w_0 (μm)
17	0.815	1.86

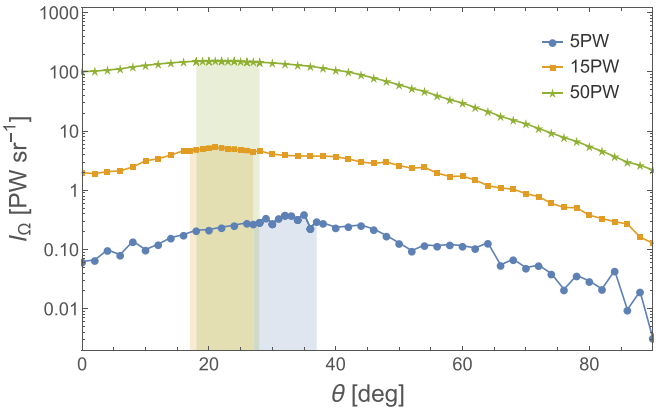

FIG. 2. Angular distribution of radiant intensity of γ-flash photons along the laser polarization axis, averaged over the two-lobe angular structure. The γ-flash is produced by the interaction with the Li solid target and focused laser pulses with peak powers of 5 PW (blue circles), 15 PW (orange squares), and 50 PW (green stars). The shaded region denotes $\beta = 10^\circ$ full-angle divergence, which maximizes the radiant intensity.

within the 10° full-angle divergence account for a large number of the highest-energy photons in the γ-flash spectrum, with lower-energy photons primarily filtered out. Calculating the laser-to-photon energy conversion efficiency for the full angular spectra (see Fig. 4), we reaffirm previous analyses demonstrating very high efficiencies for the full angular spectrum [51–68]. The proportion of laser energy converted into the $\beta = 10^\circ$ full-angle divergence is also shown.

III. NONLINEAR BREIT-WHEELER PAIR PRODUCTION

The theory of the NBW process is by now very well established and we discuss only the key features. For more details and references see [15–19]. The linear Breit-Wheeler process is the production of an electron-positron pair from two

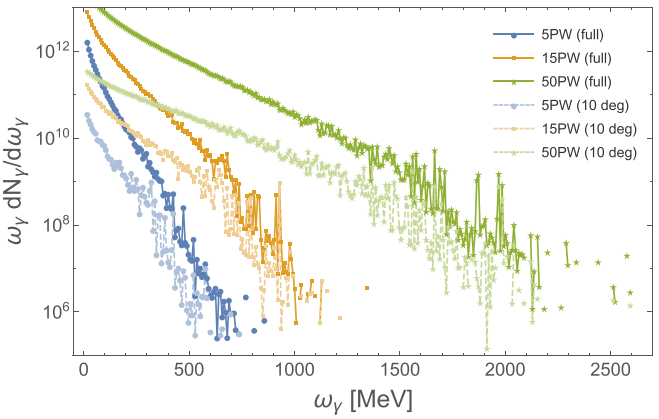

FIG. 3. The γ-flash energy spectrum $\omega_\gamma d\mathcal{N}_\gamma/d\omega_\gamma$ generated by lasers with peak powers of 5 PW (blue circles), 15 PW (orange squares), and 50 PW (green stars). Dark solid lines show the energy spectrum over all emission angles. Light dashed lines show the energy spectrum over the peak with full-angle divergence $\beta = 10^\circ$, corresponding to the respective shaded regions in Fig. 2.

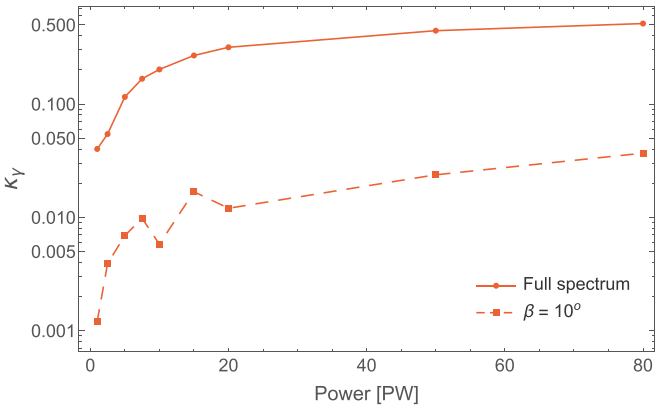

FIG. 4. Laser-to-photon energy conversion efficiency κ_γ versus laser peak power for the full spectrum (solid line) and for the photons emitted within the full-angle divergence $\beta = 10^\circ$ (dashed line).

real[2] high-energy γ photons [20]. To produce a pair, the total energy of the γ photons must exceed the minimum threshold $\omega_1 + \omega_2 \geqslant 2m$. Along with the smallness of the corresponding cross section, this has made the linear Breit-Wheeler process extremely difficult to observe experimentally [84,85]. The NBW process is a multiphoton generalization, where pairs are produced from the interaction of a single high-energy γ photon with a large number of (typically) low-energy photons which are sourced from a strong electromagnetic field [21–23]. If the field is a plane-wave pulse with dimensionless field strength ξ and wave vector k_μ, then the NBW process obeys the four-momentum conservation relation $l_\mu + \nu k_\mu = p_\mu + q_\mu$, where l_μ ($l^2 = 0$) is the momentum of the high-energy γ photon, p_μ and q_μ ($p^2 = q^2 = m^2$) are the momenta of the produced electron and positron, respectively, and ν is the proportion of energy momentum absorbed from the plane-wave background. The threshold for the NBW process can then be defined locally as $\nu \geqslant [2 + \xi^2(\phi)]/\eta_\gamma$ [86], where $\xi(\phi)$ is the local value of the intensity parameter and

$$\eta_\gamma = \frac{k \cdot l}{m^2} \tag{1}$$

is the normalized momentum of the γ photon along the direction of the colliding plane-wave field. To overcome this threshold one must have both high-energy γ photons and strong electromagnetic fields.

We consider the collision of photons with a linearly polarized plane-wave field with Gaussian envelope

$$a_\mu(\phi) = m\xi\epsilon_\mu \cos\phi e^{-4\ln(2)(\phi^2/\Phi_{\rm FWHM})^2}, \tag{2}$$

where ϕ is the phase, ϵ_μ denotes the polarization direction, and ξ is the dimensionless measure of the laser field strength [87]. The FWHM phase duration of the pulse $\Phi_{\rm FWHM}$ is related to the temporal FWHM via $\tau_{\rm FWHM} = \Phi_{\rm FWHM}\lambda_0/2c$, where λ_0 is the wavelength. To reach the highest intensities, high-power lasers must be focused. However, it is known that strong focusing can be detrimental for the NBW process (see, e.g., [39,41,43,88]). To maximize the pair yield, the influence

[2]For the case of pair production from virtual photons, typically known as the Bethe-Heitler process, see [83].

TABLE II. Constant laser parameters for colliding pulse energy E_{pairs}, which drives pair production via NBW.

τ_{FWHM} (fs)	λ_0 (μm)	w_0 (μm)
17	0.815	2.5

of transverse focusing effects should be minimized. A focused fundamental Gaussian beam propagating in the z direction with focus at $z = 0$ has a radius of curvature at some position z of $R(z) = z[1 + (z_R/z)^2]$, where $z_R = \pi w_0^2/\lambda_0$ is the Rayleigh length. As the radius of curvature becomes larger, i.e., when $(z_R/z)^2 \gg 1$, the wavefronts of the beam begin to look more like those of a plane wave. This condition can be used to define a maximum length scale $z_{\max}$ over which the focused pulse can be approximated by a plane wave. A reasonable choice would be to consider an order of magnitude in $(z_R/z)^2$, i.e., $z_{\max} = z_R/3$. This would also keep the beam radius approximately constant for $z < z_{\max}$, i.e., $w^2(z) = w_0^2[1 + (z/z_R)^2] \approx w_0^2$, such that focusing effects become minimized. Using $z_{\max}$ to set an upper bound on the laser FWHM pulse length $c\tau_{\text{FWHM}}$ gives a condition for the minimum beam waist w_0 for which the plane-wave model is valid,

$$w_0\ (\mu\text{m})\ > 0.535\sqrt{\tau_{\text{FWHM}}\ (\text{fs}) \times \lambda_0\ (\mu\text{m})}. \tag{3}$$

The wavelength and FWHM duration of the colliding pulse are chosen to match the parameters used in Sec. II: $\lambda_0 = 0.815\ \mu$m and $\tau_{\text{FWHM}} = 17$ fs. This sets a lower bound of $w_0 > 1.99\ \mu$m. Therefore, for each pulse energy E_{pairs} the beam waist will be chosen as $w_0 = 2.5\ \mu$m, i.e., $w_0 \simeq 3\lambda_0$.[3] The colliding pulse parameters are summarized in Table II.

The NBW S-matrix element for the production of an electron-positron pair with momenta (p_μ, q_μ) and spins (s, r) from the collision of a photon of momentum l_μ and polarization ε_l^μ with a plane-wave pulse is

$$S_{fi} = -ie \int d^4x\, e^{-il\cdot x} \bar{\psi}^{(-)}_{p,s}(x) \not{\varepsilon}_l \psi^{(+)}_{q,r}(x), \tag{4}$$

where e is the electron charge and the Volkov wave functions [89] for the produced electron-positron pair are

$$\bar{\psi}^{(-)}_{p,s}(x) = \exp\left(+ip\cdot x + i\int^\phi dt \frac{2p\cdot a(t) - a^2(t)}{2k\cdot p}\right)\bar{u}^s_p \times \left(1 - \frac{\not{k}\not{a}(\phi)}{2k\cdot p}\right), \tag{5}$$

$$\psi^{(+)}_{q,r}(x) = \exp\left(+iq\cdot x - i\int^\phi dt \frac{2q\cdot a(t) + a^2(t)}{2k\cdot q}\right) \times \left(1 - \frac{\not{k}\not{a}(\phi)}{2k\cdot q}\right)v^r_q, \tag{6}$$

respectively. Here $\bar{u}^s_p$ and v^r_q are free-space Dirac spinors and for any 4-vector b_μ: $\not{b} \equiv \gamma^\mu b_\mu$ with γ^μ the Dirac matrices.

Calculations are performed in light-front coordinates $x^\mu = (x^-, x^\perp, x^+)$, where $x^\pm = t \pm z$ and $x^\perp = (x, y)$. The plane wave propagates in the z direction with wave vector $k_\mu = \omega_0(1, 0, 0, 1)$ and the phase is defined as $\phi \equiv k\cdot x = \omega_0 x^-$. A generic on-shell 4-momentum p_μ is expressed in light-front variables as $p_\mu = (p_-, p_\perp, p_+)$, where $k\cdot p = 2\omega_0 p_+$, $p_\perp = (p_x, p_y)$, and the remaining component is fixed by the on-shell condition $p^2 = m^2$ as $p_- = (m^2 + p_\perp^2)/4p_+$. Integrals over $(x^\perp, x^+)$ in Eq. (4) yield momentum-conserving δ functions. The differential probability can then be found by taking the squared modulus of S_{fi}, averaging (summing) over initial (final) spins, and integrating over the electron momenta p_μ. We are specifically interested in the interaction of MeV to GeV photons with multipetawatt, multicycle laser pulses, where the dimensionless intensity parameter $\xi \gg 1$. As such, we are within the regime of validity[4] of the locally constant field approximation (LCFA), which gives the angularly resolved differential probability

$$\frac{d^3\mathsf{P}_{\text{LCFA}}}{dr\,d\eta_q\,d\psi} = \frac{\alpha r}{\pi\eta_\gamma^2}\int d\phi\ \text{Ai}[\bar{z}(\phi)] \times \left[z(\phi) + \left(\frac{(\eta_\gamma - \eta_q)^2 + \eta_q^2}{\eta_q(\eta_\gamma - \eta_q)}\right)\bar{z}(\phi)\right], \tag{7}$$

where $\alpha = e^2/4\pi$ is the fine-structure constant. The argument of the Airy function $\text{Ai}[\bar{z}(\phi)]$ is

$$\bar{z}(\phi) = z(\phi)\left(1 + r^2 + \frac{|a_\perp(\phi)|^2}{m^2} + \frac{2r|a_\perp(\phi)|\cos\psi}{m}\right), \tag{8}$$

where

$$z(\phi) = \left(\frac{1}{\chi_\gamma(\phi)}\frac{\eta_\gamma^2}{\eta_q(\eta_\gamma - \eta_q)}\right)^{2/3} \tag{9}$$

is defined in terms of the quantum nonlinearity parameter of the photon

$$\chi_\gamma(\phi) = \frac{\eta_\gamma|a'_\perp(\phi)|}{m}, \tag{10}$$

where $a'_\perp(\phi) \equiv da_\perp(\phi)/d\phi$.

The probability is compactly parametrized by three parameters (η_q, r, ψ), where

$$\eta_q = \frac{k\cdot q}{m^2} \tag{11}$$

is the normalized momentum of the positron along the direction of the colliding plane wave $r = |r_\perp|$, where

$$r_\perp = \frac{q_\perp - \frac{\eta_q}{\eta_\gamma}l_\perp}{m} \tag{12}$$

is a measure of the positron momentum in the plane perpendicular to the direction of the laser and $\psi \in [0, 2\pi)$ is the azimuthal emission angle in the perpendicular plane, i.e.,

[3]Blackburn and Marklund [39] demonstrated that for short pulses ($\tau_{\text{FWHM}} < 20$ fs) and small collision angles focusing effects only contribute a small change to the total pair-production probability for $2 < w_0/\lambda_0 < 10$. This is in agreement with our simple approximations and choice of parameters.

[4]For discussions of the regime of validity of the LCFA see [15,90,91] and for extensions or alternatives see [86,92–94].

we could also write $r_\perp = r\{\cos\psi, \sin\psi\}$. When the perpendicular momentum of the photon can be neglected, $q_\perp \gg (\eta_q/\eta_\gamma)l_\perp$, and the energy of the produced positron $E_q \gg m$, then $r \approx (E_q/m)\sin\vartheta$ and $\eta_q \approx (\omega_0 E_q/m^2)(1+\cos\vartheta)$, where ϑ is the emission angle relative to the colliding laser propagation axis (chosen here as the z axis). Thus, for small emission angles $\vartheta \ll 1$, $r \approx E_q\vartheta/m$ and $\eta_q \approx 2\omega_0 E_q/m$ and we can readily interpret the pair (r, η_q) as a parametrization of the positron's emission angle and energy.

Integrating Eq. (7) returns the total probability $\mathsf{P}_{\mathrm{LCFA}}$ for the NBW process by a single photon with momentum l_μ. However, in certain regimes $\mathsf{P}_{\mathrm{LCFA}}$ can exceed unity and its interpretation as a probability becomes ambiguous. This is due to higher-order loop effects being neglected. These can be included by solving the Schwinger-Dyson equations to arrive at photon wave functions which demonstrate an exponential decay [95]. One can then define a decay probability

$$\mathsf{W} = 1 - \exp(-\mathsf{P}_{\mathrm{LCFA}}), \tag{13}$$

in which $\mathsf{P}_{\mathrm{LCFA}}$ now has the interpretation as the decay exponent for a photon with momentum l_μ propagating through the laser pulse (see, e.g., [41,95–97]). When $\mathsf{P}_{\mathrm{LCFA}} \ll 1$, then $\mathsf{W} \approx \mathsf{P}_{\mathrm{LCFA}}$ and $\mathsf{P}_{\mathrm{LCFA}}$ can again be interpreted as a probability.

IV. PAIRS FROM γ FLASH

Photons are produced at the target rear surface and are spread in the angular plane (cf. Fig. 2). As discussed in Sec. II we consider photons within the full-angle divergence of $\beta = 10^\circ$ for which the radiant intensity of the photons is maximized. These photons will propagate a distance d to the colliding laser focus, expanding from the rear target surface as a spherical shell. The distance d will typically be of $O(10\,\mathrm{cm})$ and the spherical shell of photons within the full-angle divergence $\beta = 10^\circ$ will have a large radius of curvature and transverse size relative to the colliding laser-beam waist, $w_0 \sim O(\mu\mathrm{m})$. The beam of photons which collide with the pulse can therefore be well approximated as a flat disk propagating from the target point source and the perpendicular momentum of the photons can be neglected, i.e., $l_\perp \approx 0$, such that the photons collide approximately head-on with the counterpropagating laser pulse. After propagating a distance d the photon beam will have an area $A_{\mathrm{flash}} = \pi d^2 \tan^2(\beta/2)$. The photons will then collide with a counterpropagating laser pulse with a focal spot area $A_{\mathrm{laser}} = \pi w_0^2$, where w_0 is the beam waist. Given a total number of photons $\mathcal{N}_\gamma$ within the full-angle divergence β, the total number of photons within the laser focal spot, focused at the distance d, will be[5]

$$\frac{\mathcal{N}_\gamma w_0^2}{d^2\tan^2(\beta/2)}. \tag{14}$$

[5]The validity of Eq. (14) requires $A_{\mathrm{flash}} > A_{\mathrm{laser}}$, which for $\beta = 10^\circ$ is satisfied when $d \gtrsim 11 w_0$.

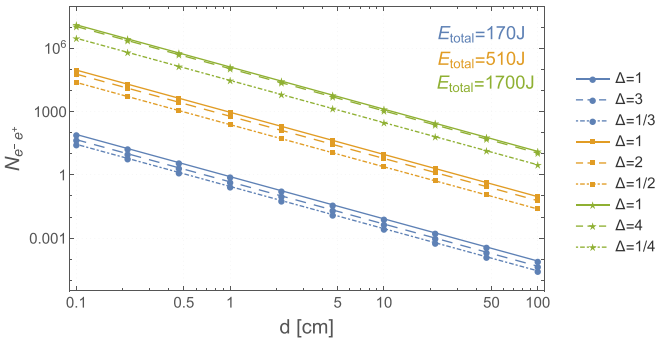

FIG. 5. Total number of produced pairs $\mathcal{N}_{e^-e^+}$ as a function of photon-laser interaction point distance d calculated with Eq. (15) for $E_{\mathrm{total}} = 170$ J (blue circles), $E_{\mathrm{total}} = 510$ J (orange squares), and $E_{\mathrm{total}} = 1700$ J (green stars). The legend gives the values of the ratio Δ [cf. Eq. (16)].

Then the total number of pairs generated from the collision of the photon beam with the colliding laser is

$$\mathcal{N}_{e^-e^+} = \frac{w_0^2}{d^2\tan^2(\beta/2)}\int_0^\infty d\omega_\gamma \mathsf{W}(\omega_\gamma)\frac{d\mathcal{N}_\gamma(\omega_\gamma)}{d\omega_\gamma}, \tag{15}$$

where $\mathsf{W}(\omega_\gamma)$ is defined by Eq. (13) and $d\mathcal{N}_\gamma(\omega_\gamma)/d\omega_\gamma$ is the differential number of photons with energy ω_γ.

At a high-power laser facility, the key constraining parameter is the deliverable pulse energy. Current and upcoming petawatt and multipetawatt laser facilities typically have deliverable pulse energies of $E_{\mathrm{total}} \sim$ 30–1500 J, with durations $\tau_{\mathrm{FWHM}} \sim$ 15–30 fs [1], with notable exceptions such as the 10-PW laser system at ELI Beamlines [8], which will have a long pulse duration of 150 fs. The proposed scheme (Fig. 1) takes the total available laser energy and splits this into two $E_{\mathrm{total}} = E_{\mathrm{flash}} + E_{\mathrm{pairs}}$, where the pulse with energy E_{flash} drives the photon production via the γ-flash mechanism and the pulse with energy E_{pairs} collides with those photons to produce pairs. We will consider three different cases for the total available laser energy $E_{\mathrm{total}} = (170, 510, 1700)$ J and further consider different ratios

$$\Delta = \frac{E_{\mathrm{flash}}}{E_{\mathrm{pairs}}} \tag{16}$$

to find the optimal splitting of the total available laser energy for producing pairs. Both pulses have a FWHM duration $\tau_{\mathrm{FWHM}} = 17$ fs such that the total available power for each case is $P_{\mathrm{total}} = (10, 30, 100)$ PW. Current state-of-the-art technology has fueled the development of a number of 10-PW-class laser facilities [7–11], with future facilities (see, e.g., [13,14]) aiming to break the 100-PW peak power threshold (see also [98,99]. Our considerations will therefore explore the feasibility of using γ-flash photons to observe nonlinear Breit-Wheeler pair production at current-, next-, and future-generation high-power laser facilities.

In Fig. 5 we plot the total number of pairs produced as the distance d is increased, using Eq. (15). The corresponding values of the peak intensities for the different total energies E_{total} and ratios Δ used in Fig. 5 are outlined in Table III. Comparing the total number of pairs produced for different values of the splitting ratio Δ at fixed E_{total} and d suggests that the

TABLE III. Peak intensity parameters used to calculate the total number of electron-positron pairs in Fig. 5. The constant parameters for the driving and colliding laser pulses are given in Tables I and II, respectively. The intensity of each pulse is given both in terms of the dimensionless intensity parameters ξ_{flash} and ξ_{pairs} and the equivalent power per unit area I_{flash} and I_{pairs}.

E_{total} (J)	Δ	ξ_{flash}	ξ_{pairs}	I_{flash} (W cm^{-2})	I_{pairs} (W cm^{-2})
	1	149	111	4.6×10^{22}	2.5×10^{22}
170	3	183	79	6.9×10^{22}	1.27×10^{22}
	1/3	106	136	2.3×10^{22}	3.8×10^{22}
	1	259	193	1.4×10^{23}	7.6×10^{22}
510	2	299	157	1.84×10^{23}	5.1×10^{22}
	1/2	211	222	9.2×10^{22}	1.0×10^{23}
	1	473	352	4.6×10^{23}	2.5×10^{23}
1700	4	598	222	7.36×10^{23}	1.0×10^{23}
	1/4	299	445	1.84×10^{23}	4.0×10^{23}

number of pairs will be maximized when there is an equal split of the total energy into the beams which drive the γ-flash photon generation and pair production via the NBW process, i.e., when $\Delta = 1$. For the lowest total laser energy $E_{\text{total}} = 170$ J, we find $\mathcal{N}_{e^-e^+}^{\Delta=1}/\mathcal{N}_{e^-e^+}^{\Delta=3} \approx 1.8$ and $\mathcal{N}_{e^-e^+}^{\Delta=1}/\mathcal{N}_{e^-e^+}^{\Delta=1/3} \approx 2.9$. At the intermediate energy $E_{\text{total}} = 510$ J, we see a similar scaling between the ratios of the number of pairs with each value of Δ, with $\mathcal{N}_{e^-e^+}^{\Delta=1}/\mathcal{N}_{e^-e^+}^{\Delta=2} \approx 1.6$ and $\mathcal{N}_{e^-e^+}^{\Delta=1}/\mathcal{N}_{e^-e^+}^{\Delta=1/2} \approx 3.9$. Finally, at the highest energy $E_{\text{total}} = 1700$J, we find $\mathcal{N}_{e^-e^+}^{\Delta=1}/\mathcal{N}_{e^-e^+}^{\Delta=4} \approx 1.2$ and $\mathcal{N}_{e^-e^+}^{\Delta=1}/\mathcal{N}_{e^-e^+}^{\Delta=1/4} \approx 4.3$.

In the process of producing photons via the γ-flash mechanism, electrons and positrons are also created and emitted from the target rear surface (see, e.g., [51,53,58,60,64]). The positrons are produced by high-energy photons inside the target such that their energy and angular distribution are comparable to the emitted γ-flash photons, while electrons are produced both by pair production and by direct acceleration of target electrons by the irradiating laser pulse. To minimize the background of charged particles an experiment would separate these from the photons using magnetic deflection or other methods. The photon propagation distance d therefore needs to be sufficiently large to allow for this background of particles to be filtered from the photons. For example, a permanent magnet of length L and field strength B can deflect an electron or positron propagating perpendicular to to the magnetic field with energy $\mathcal{E}$ by an angle δ (deg) $\simeq 0.17L$ (cm)B (T)$\mathcal{E}^{-1}$ (GeV). To ensure the background of charged particles at the focus of the colliding laser (energy E_{pairs}) is minimized, the deflection angle of particles propagating with the γ-flash photons should satisfy $\delta \gg \delta_{\text{min}}$, where δ_{min} (deg) $\simeq 6\times10^{-3}w_0$ (μm)d^{-1} (cm). This corresponds to a magnet of length L (cm) $\gg 0.03w_0$ (μm)$\mathcal{E}$ (GeV)d^{-1} (cm)B^{-1} (T). Considering a photon propagation distance of $d = 10$ cm, deflecting a positron, with energy $\mathcal{E} = 3$ GeV, with a magnet of field strength $B = 1$ T away from the colliding laser focus of $w_0 = 2.5$ μm would require $L \gg 0.02$ cm. A large number of background particles could therefore be removed with, for example, an $L = 5$ cm neodymium magnet.

With the colliding laser focus at $d = 10$ cm and using the optimal beam splitting ratio of $\Delta = 1$, the total number of pairs produced per shot for the different energies $E_{\text{total}} = (170, 510, 1700)$ J is $\mathcal{N}_{e^-e^+} \sim (0.01, 10, 1300)$, respectively. A typical high-power laser has a repetition rate of the order of 0.1–10 Hz [1]. This means that with an interaction distance $d = 10$ cm and nominal repetition rate of 0.1 Hz, an experiment could expect to produce approximately five pairs per hour,[6] with the 10-PW equivalent system, increasing to approximately 10^5 pairs per hour with 100 PW. If the interaction distance could be further reduced to $d = 1$ cm, the number of pairs per shot increases substantially to $\mathcal{N}_{e^-e^+} \sim (1, 1000, 10^5)$ pairs per shot, respectively.

For the three total laser energies E_{total} with the optimal splitting $\Delta = 1$, Fig. 6 compares the differential number of pairs produced $d\mathcal{N}_{e^-e^+}/d\omega_\gamma$ (light dashed line) with the differential number of photons which interact with the colliding laser $d\mathcal{N}_\gamma/d\omega_\gamma$ (dark solid line). The NBW process becomes more probable as $\chi_\gamma \gtrsim 1$ and so in each case the value of the photon energy ω_γ which satisfies $\max[\chi_\gamma] = \eta_\gamma \xi_{\text{pairs}} = 1$ is shown (black dashed line). For the lowest considered total laser energy $E_{\text{total}} = 170$ J, one can see that only a small portion of the photons which collide with the secondary pulse are converted into electron-positron pairs. The peak dimensionless intensity of the colliding laser in this case is $\xi_{\text{pairs}} \approx 111$, which means only photons with energies $\omega_\gamma \gtrsim 771$ MeV will experience peak values of the quantum nonlinearity parameter $\max[\chi_\gamma] \gtrsim 1$. This corresponds to only approximately 10^{-5}% of the total number of photons in the spectrum, or equivalently approximately 10^{-4}% of the total energy. For the case $E_{\text{total}} = 510$ J, the peak dimensionless intensity increases to $\xi_{\text{pairs}} \approx 193$ and $\max[\chi_\gamma] \gtrsim 1$ is satisfied for photons with $\omega_\gamma \gtrsim 445$ MeV, which accounts for approximately 0.2% of the total number and approximately 2.5% of the total energy. This then leads to a corresponding increase in the number of pairs produced. The number of pairs then increases significantly for the highest energy case $E_{\text{total}} = 1700$ J, where approximately 10% of the total number of photons (approximately 35% of the total spectrum energy) satisfy the condition $\omega_\gamma \gtrsim 244$ MeV which is required for $\max[\chi_\gamma] \gtrsim 1$ with the dimensionless intensity parameter $\xi_{\text{flash}} \approx 352$.

Turning now to the properties of the produced positrons, Fig. 7 shows the double differential spectra in the physical variables (ϑ, E_q), i.e., $d^2\mathcal{N}_{e^-e^+}/d\vartheta dE_q$, for the three cases of total laser energy E_{total}, with $\Delta = 1$. Similarly, Fig. 8 shows the corresponding single differential energy and angular spectra $d\mathcal{N}_{e^-e^+}/dE_q$ and $d\mathcal{N}_{e^-e^+}/d\vartheta$, respectively. The structure of the NBW probability (7) causes suppression of the pair production except around sharply peaked values of the dimensionless variable r. Increasing the total available laser energy leads to larger values of r being attained by the produced electron-positron pairs, due to the stronger transverse field which they experience. From $r \approx (E_q/m)\sin\vartheta$ we can see that increasing r means increasing the energy of the produced

[6]This is comparable to the estimated number of NBW pairs which will be produced per hour at a proposed experiment with the CALA laser [43,100], which will use LWFA electrons to generate photon production via bremsstrahlung (cf. Sec. I).

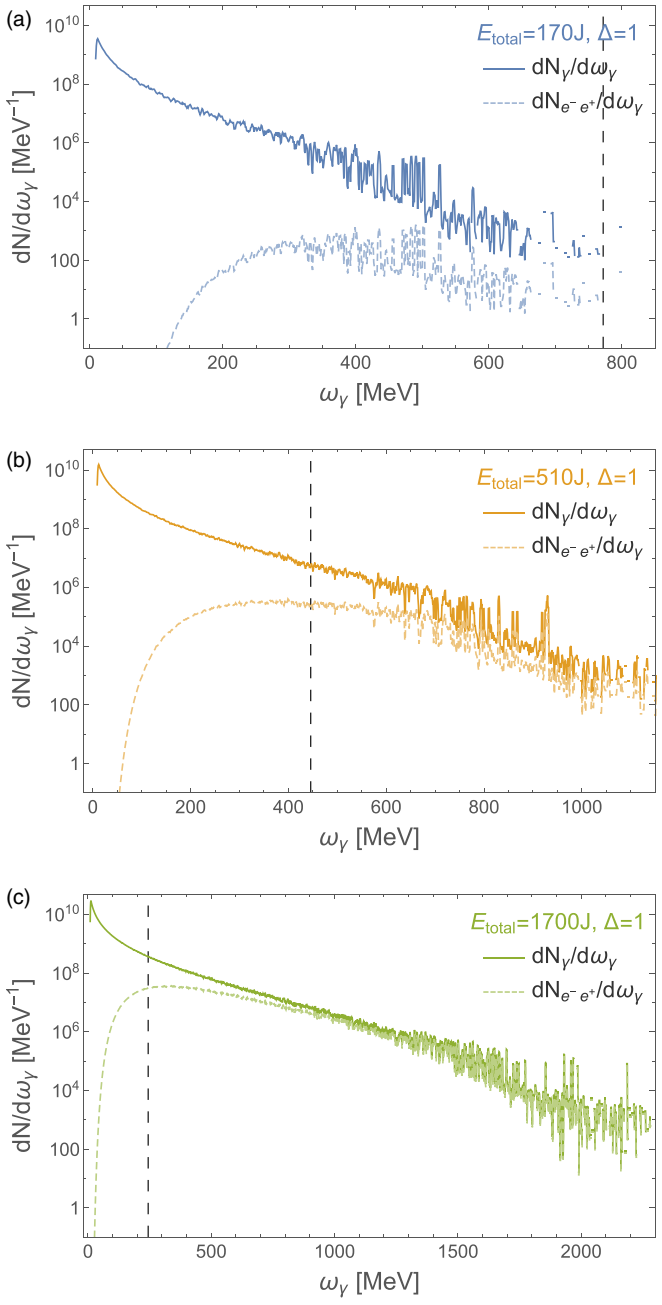

FIG. 6. Comparison of initial photon spectrum $d\mathcal{N}_\gamma/d\omega_\gamma$ (solid line) with the differential number of pairs $d\mathcal{N}_{e^-e^+}/d\omega_\gamma$ (dashed line) for (a) $E_{\text{total}} = 170$ J and $\Delta = 1$, (b) $E_{\text{total}} = 510$ J and $\Delta = 1$, and (c) $E_{\text{total}} = 1700$ J and $\Delta = 1$. Black dashed lines denote the value of ω_γ for which $\max[\chi_\gamma] = \eta_\gamma \xi_{\text{pairs}} = 1$.

positrons E_q and/or increasing their emission angle ϑ. The double differential spectra in Fig. 7 follow curved lines of approximately constant r, i.e., $\vartheta \approx \sin^{-1}(mr/E_q)$. Increasing the energy of the driving laser pulse increases both the maximum energy of the γ-flash photons and the overall number of photons, particularly those of lower energy (cf. Fig. 3). As the energy of the secondary colliding pulse increases, more of the lower-energy photons can be converted into electron-positron pairs due to the threshold energy for $\max[\chi_\gamma] \gtrsim 1$ being reduced (see Fig. 6). This in turn leads to more low-energy electron-positron pairs being produced, which pushes the peak in the energy spectrum to lower values of the energy E_q as the total available laser energy E_{total} is increased, as shown in Figs. 8(a)–8(c). Furthermore, low-energy positrons are more strongly influenced by the electromagnetic field of the colliding laser and are emitted at larger emission angles ϑ (cf. Fig. 7). This leads to a broadening of the single differential angular spectra $d\mathcal{N}_{e^-e^+}/d\vartheta$ as E_{total} increases, as shown in Figs. 8(d)–8(f).

V. SUMMARY AND OUTLOOK

Current- and next-generation high-power laser facilities will be capable of delivering multipetawatt peak power laser pulses for studying strong-field QED processes in the laboratory. Here we have explored the feasibility of experimentally observing the nonlinear Breit-Wheeler process using a simple and efficient two-stage setup whereby high-energy photons produced by irradiating an overdense plasma with a laser pulse collide with a secondary laser pulse to produce electron-positron pairs.

Photons produced by the γ-flash mechanism have an angular spread, producing a double-lobe pattern. We found the optimal angle for the secondary collision by maximizing the radiant intensity of the γ-flash photons and showed that the photons within a full-angle divergence of $\beta = 10^\circ$ around this optimal angle accounted for a large proportion of the highest-energy γ-flash photons (cf. Fig. 3).

Considering three different cases for the available laser energy $E_{\text{laser}} = (170, 510, 1700)$ J, which for pulses with duration 17 fs corresponds to powers $P = (10, 30, 100)$ PW, we demonstrated that the optimal splitting between the laser energy dedicated to producing photons via the γ-flash mechanism, E_{flash}, and the energy used in the secondary pulse responsible for converting photons to pairs via the nonlinear Breit-Wheeler mechanism, E_{pairs}, was $\Delta = E_{\text{flash}}/E_{\text{pairs}} = 1$. In each case this optimized the number of electron-positron pairs produced. By locating the focus of the secondary laser pulse with energy E_{pairs} at a distance $d = 10$ cm from the rear surface, our findings suggest that with current capabilities on the order of 0.01, pairs could be produced per shot with $E_{\text{total}} = 170$ J and next-generation facilities capable of reaching 100 PW, with total available energy $E_{\text{total}} = 1700$ J, could see as many as 1200 pairs being produced per shot.

As well as calculating the total number of produced pairs, we have considered the energy and angular spectra, showing that the broadness of the γ-flash energy spectrum produces positrons with a strong peak with a high-energy tail. For lower laser energies or powers, the positrons are strongly emitted in the seed photon direction, but for larger energies or powers they can develop a larger transverse momentum component. This is due to the higher laser energies allowing lower-energy photons in the initial spectrum to decay into pairs, which are then more strongly kicked in the transverse plane by the laser.

Having demonstrated the feasibility of using the γ-flash mechanism to generate seed photons for nonlinear Breit-Wheeler pair production, there are a number of possible routes which could be explored in future work. There are several optimizations which could be explored, in both the γ-flash photon-production stage and the nonlinear Breit-Wheeler

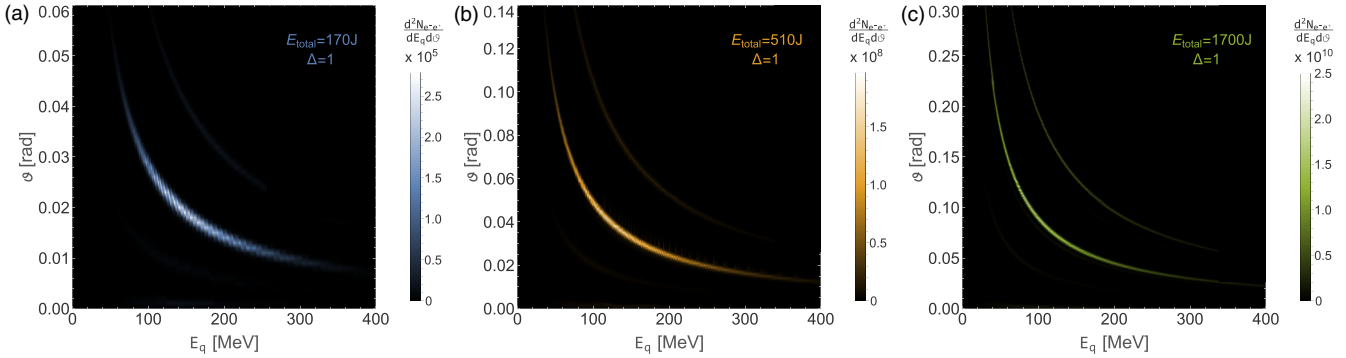

FIG. 7. Double differential spectra $d^2\mathcal{N}_{e^-e^+}/d\vartheta dE_q$ for (a) $E_{\text{total}} = 170$ J, (b) $E_{\text{total}} = 510$ J, and (c) $E_{\text{total}} = 1700$ J.

stage. In the photon-production stage we have kept the target thickness, pulse duration, and focal spot size constant for each pulse energy E_{flash}. Related work which instead produces photons via bremsstrahlung from a high-energy electron colliding with a solid target [39] determined an optimal target thickness for maximizing the number of electron-positron pairs produced in the second stage where the photons collide with an intense laser pulse. We leave for future work the exploration of whether an optimal target thickness can also be determined in the γ-flash case. This could lead to significant optimizations on two fronts. First is by increasing the energy and number of photons produced, which will directly increase the number of pairs which can be obtained in the second stage. Second, increasing the target thickness can reduce the number of secondary charged particles produced by the γ-flash mechanism. By minimizing the number of background particles through an optimal thickness of the target and/or the duration of the laser pulse incident on the target, one could decrease the distance d to the interaction point where the secondary laser pulse is focused. Since the total number of pairs produced scales with d^{-2}, this could lead to significant increases in the total number of pairs produced. For example, for a distance $d = 1$ cm considered above, the estimated number of pairs per shot for the total laser energies $E_{\text{total}} = (170, 510, 1700)$ J are as high as $\mathcal{N}_{e^-e^+} \sim (1, 1000, 10^5)$.

Another optimization which could be explored further with regard to the photon-generation stage is the use of alternative laser polarizations to reduce the divergence of the photon beam. Here we have used a linearly polarized laser pulse, which produces the characteristic double-lobe angular intensity pattern in the γ-flash photons, but recent work [60] utilizing a radially polarized beam has indicated a much lower divergence of the photon beam. This could lead to a significantly larger number of photons propagating to the focus of the secondary laser pulse, which could help increase the total number of pairs produced via the nonlinear Breit-Wheeler mechanism.

With regard to the second stage where the γ-flash photons collide with the second laser pulse of energy E_{pairs}, there are further improvements which are left for exploration in future work. First, we have chosen the beam waist of the secondary laser pulse to minimize the influence of focusing effects and modeled the laser pulse as a plane wave with Gaussian temporal profile. This means that the highest intensities which the photons experience in the laser pulse are not as high as could be achieved with stronger focusing. How-

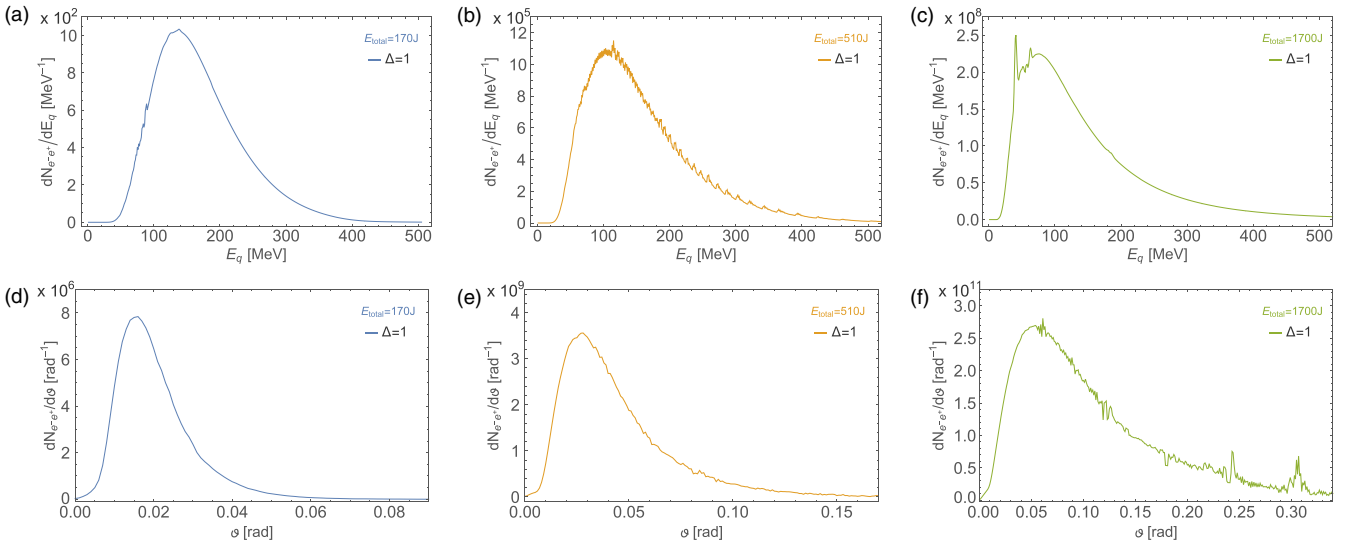

FIG. 8. Single differential spectra: (a)–(c) energy spectra $d\mathcal{N}_{e^-e^+}/dE_q$ and (d)–(f) angular spectra $d\mathcal{N}_{e^-e^+}/d\vartheta$ for (a) and (d) $E_{\text{total}} = 170$ J and $\Delta = 1$, (b) and (e) $E_{\text{total}} = 510$ J and $\Delta = 1$, and (c) and (f) $E_{\text{total}} = 1700$ J and $\Delta = 1$.

ever, it is known that focusing effects can have a detrimental effect on the number of pairs produced (see, e.g., [39,41]). Focusing effects can be included for high-energy photons and high field strengths in the probabilities using, for example, a high-energy WKB approach [88]. We leave the interplay between the competing effects of reaching high field strength and minimizing the detrimental effects of focusing for future work. Including focusing effects will also allow the effect of pulse duration to be considered beyond the plane-wave model.

As noted previously, one of the parameters with the highest impact on the number of pairs produced is d, which is the distance from the source of the γ-flash photons to the focal spot of the secondary laser pulse. Depending on the background of secondary charged particles produced in the γ-flash mechanism, this distance may need to be sufficiently large to allow for magnetic deflection of these particles using stationary magnets or other techniques (see, e.g., [101]). The pairs produced via the nonlinear Breit-Wheeler stage of the proposed setup have an angular spread. In light of this, it may be possible to to find a region in the angular plane where the background of charged particles is minimized and the signal of nonlinear Breit-Wheeler pairs can be easily detected. This would allow the distance d to be reduced without the need of magnetically deflecting the background particles. This will require more accurate modeling of the final distribution of background particles at the detection region, for example, by using additional simulations with QED PIC codes or Monte Carlo codes such as FLUKA [102], GEANT4 [103], or similar. This is left for future work.

ACKNOWLEDGMENT

This work was supported by the project Advanced Research using High Intensity Laser Produced Photons and Particles (ADONIS) (Project No. CZ.02.1.01/0.0/0.0/16_019/0000789) from the European Regional Development Fund.

[1] C. N. Danson, C. Haefner, J. Bromage, T. Butcher, J.-C. F. Chanteloup, E. A. Chowdhury, A. Galvanauskas, L. A. Gizzi, J. Hein, D. I. Hillier *et al.*, High Power Laser Sci. Eng. **7**, e54 (2019).

[2] H. Kiriyama, A. S. Pirozhkov, M. Nishiuchi, Y. Fukuda, K. Ogura, A. Sagisaka, Y. Miyasaka, M. Mori, H. Sakaki, N. P. Dover *et al.*, Opt. Lett. **43**, 2595 (2018).

[3] J. H. Sung, H. W. Lee, J. Y. Yoo, J. W. Yoon, C. W. Lee, J. M. Yang, Y. J. Son, Y. H. Jang, S. K. Lee, and C. H. Nam, Opt. Lett. **42**, 2058 (2017).

[4] J. W. Yoon, Y. G. Kim, I. W. Choi, J. H. Sung, H. W. Lee, S. K. Lee, and C. H. Nam, Optica **8**, 630 (2021).

[5] J. Nees, A. Maksimchuk, G. Kalinchenko, B. Hou, Y. Ma, P. Campbell, A. McKelvey, L. Willingale, I. Jovanovic, C. Kuranz *et al.*, *Conference on Lasers and Electro-Optics* (Optica, Washington, DC, 2021), paper JTu3A.10.

[6] C. Hernandez-Gomez, S. P. Blake, O. Chekhlov, R. J. Clarke, A. M. Dunne, M. Galimberti, S. Hancock, R. Heathcote, P. Holligan, A. Lyachev *et al.*, J. Phys.: Conf. Ser. **244**, 032006 (2010).

[7] D. Papadopoulos, J.P. Zou, C. Le Blanc, G. Chériaux, P. Georges, F. Druon, G. Mennerat, P. Ramirez, L. Martin, A. Fréneaux *et al.*, High Power Laser Sci. Eng. **4**, e34 (2016).

[8] S. Weber, S. Bechet, S. Borneis, L. Brabec, M. Bučka, E. Chacon-Golcher, M. Ciappina, M. DeMarco, A. Fajstavr, K. Falk *et al.*, Matter Radiat. Extremes **2**, 149 (2017).

[9] S. Gales, K. A. Tanaka, D. L. Balabanski, F. Negoita, D. Stutman, O. Tesileanu, C. A. Ur, D. Ursescu, I. Andrei, S. Ataman *et al.*, Rep. Prog. Phys. **81**, 094301 (2018).

[10] J. Bromage, S.-W. Bahk, M. Bedzyk, I. A. Begishev, S. Bucht, C. Dorrer, C. Feng, C. Jeon, C. Mileham, R. G. Roides *et al.*, High Power Laser Sci. Eng. **9**, e63 (2021).

[11] Z. Gan, L. Yu, C. Wang, Y. Liu, Y. Xu, W. Li, S. Li, L. Yu, X. Wang, X. Liu *et al.*, *The Shanghai Superintense Ultrafast Laser Facility (SULF) Project* (Springer International, Cham, 2021), pp. 199–217.

[12] J. D. Zuegel, S.-W. Bahk, I. A. Begishev, J. Bromage, C. Dorrer, A. V. Okishev, and J. B. Oliver, *CLEO: 2014* (Optica, Washington, DC, 2014), paper JTh4L.4.

[13] I. Mukhin, A. Soloviev, E. Perevezentsev, A. Shaykin, V. Ginzburg, I. Kuzmin, M. Mart'yanov, I. Shaikin, A. Kuzmin, S. Mironov *et al.*, Quantum Electron. **51**, 759 (2021).

[14] B. Shen, Z. Bu, J. Xu, T. Xu, L. Ji, R. Li, and Z. Xu, Plasma Phys. Control. Fusion **60**, 044002 (2018).

[15] V. I. Ritus, J. Sov. Laser Res. **6**, 497 (1985).

[16] F. Ehlotzky, K. Krajewska, and J. Z. Kamiński, Rep. Prog. Phys. **72**, 046401 (2009).

[17] A. Di Piazza, C. Müller, K. Z. Hatsagortsyan, and C. H. Keitel, Rev. Mod. Phys. **84**, 1177 (2012).

[18] P. Zhang, S. S. Bulanov, D. Seipt, A. V. Arefiev, and A. G. R. Thomas, Phys. Plasmas **27**, 050601 (2020).

[19] A. Fedotov, A. Ilderton, F. Karbstein, B. King, D. Seipt, H. Taya, and G. Torgrimsson, arXiv:2203.00019.

[20] G. Breit and J. A. Wheeler, Phys. Rev. **46**, 1087 (1934).

[21] H. R. Reiss, J. Math. Phys. **3**, 59 (1962).

[22] A. Nikishov and V. Ritus, Sov. Phys. JETP **19**, 529 (1964).

[23] V. Yakovlev, Sov. Phys. JETP **22**, 223 (1966).

[24] F. Sauter, Z. Phys. **69**, 742 (1931).

[25] W. Heisenberg and H. Euler, Z. Phys. **98**, 714 (1936).

[26] J. Schwinger, Phys. Rev. **82**, 664 (1951).

[27] A. Gonoskov, T. G. Blackburn, M. Marklund, and S. S. Bulanov, Rev. Mod. Phys. **94**, 045001 (2022).

[28] E. Esarey, S. K. Ride, and P. Sprangle, Phys. Rev. E **48**, 3003 (1993).

[29] L. S. Brown and T. W. B. Kibble, Phys. Rev. **133**, A705 (1964).

[30] I. Goldman, Phys. Lett. **8**, 103 (1964).

[31] F. V. Hartemann, W. J. Brown, D. J. Gibson, S. G. Anderson, A. M. Tremaine, P. T. Springer, A. J. Wootton, E. P. Hartouni, and C. P. J. Barty, Phys. Rev. ST Accel. Beams **8**, 100702 (2005).

[32] B. King and S. Tang, Phys. Rev. A **102**, 022809 (2020).

[33] S. Tang, B. King, and H. Hu, Phys. Lett. B **809**, 135701 (2020).

[34] S. Chen, N. D. Powers, I. Ghebregziabher, C. M. Maharjan, C. Liu, G. Golovin, S. Banerjee, J. Zhang, N. Cunningham, A. Moorti *et al.*, Phys. Rev. Lett. **110**, 155003 (2013).

[35] G. Sarri, D. J. Corvan, W. Schumaker, J. M. Cole, A. Di Piazza, H. Ahmed, C. Harvey, C. H. Keitel, K. Krushelnick, S. P. D. Mangles *et al.*, Phys. Rev. Lett. **113**, 224801 (2014).

[36] W. Yan, C. Fruhling, G. Golovin, D. Haden, J. Luo, P. Zhang, B. Zhao, J. Zhang, C. Liu, M. Chen *et al.*, Nat. Photon. **11**, 514 (2017).

[37] J. Galy, M. Maučec, D. J. Hamilton, R. Edwards, and J. Magill, New J. Phys. **9**, 23 (2007).

[38] K. W. D. Ledingham and W. Galster, New J. Phys. **12**, 045005 (2010).

[39] T. G. Blackburn and M. Marklund, Plasma Phys. Control. Fusion **60**, 054009 (2018).

[40] H. Abramowicz, U. Acosta, M. Altarelli, R. Aßmann, Z. Bai, T. Behnke, Y. Benhammou, T. Blackburn, S. Boogert, O. Borysov *et al.*, Eur. Phys. J.: Spec. Top. **230**, 2445 (2021).

[41] A. Mercuri-Baron, M. Grech, F. Niel, A. Grassi, M. Lobet, A. D. Piazza, and C. Riconda, New J. Phys. **23**, 085006 (2021).

[42] A. Eckey, A. B. Voitkiv, and C. Müller, Phys. Rev. A **105**, 013105 (2022).

[43] A. Golub, S. Villalba-Chávez, and C. Müller, Phys. Rev. D **105**, 116016 (2022).

[44] A. Sampath, X. Davoine, S. Corde, L. Gremillet, M. Gilljohann, M. Sangal, C. H. Keitel, R. Ariniello, J. Cary, H. Ekerfelt *et al.*, Phys. Rev. Lett. **126**, 064801 (2021).

[45] A. Matheron *et al.*, arXiv:2209.14280.

[46] T. Tajima and J. M. Dawson, Phys. Rev. Lett. **43**, 267 (1979).

[47] E. Esarey, C. B. Schroeder, and W. P. Leemans, Rev. Mod. Phys. **81**, 1229 (2009).

[48] A. J. Gonsalves, K. Nakamura, J. Daniels, C. Benedetti, C. Pieronek, T. C. H. de Raadt, S. Steinke, J. H. Bin, S. S. Bulanov, J. van Tilborg *et al.*, Phys. Rev. Lett. **122**, 084801 (2019).

[49] C. Bula, K. T. McDonald, E. J. Prebys, C. Bamber, S. Boege, T. Kotseroglou, A. C. Melissinos, D. D. Meyerhofer, W. Ragg, D. L. Burke *et al.*, Phys. Rev. Lett. **76**, 3116 (1996).

[50] C. Bamber, S. J. Boege, T. Koffas, T. Kotseroglou, A. C. Melissinos, D. D. Meyerhofer, D. A. Reis, W. Ragg, C. Bula, K. T. McDonald *et al.*, Phys. Rev. D **60**, 092004 (1999).

[51] C. P. Ridgers, C. S. Brady, R. Duclous, J. G. Kirk, K. Bennett, T. D. Arber, A. P. L. Robinson, and A. R. Bell, Phys. Rev. Lett. **108**, 165006 (2012).

[52] T. Nakamura, J. K. Koga, T. Z. Esirkepov, M. Kando, G. Korn, and S. V. Bulanov, Phys. Rev. Lett. **108**, 195001 (2012).

[53] C. S. Brady, C. P. Ridgers, T. D. Arber, and A. R. Bell, Phys. Plasmas **21**, 033108 (2014).

[54] J.-X. Li, K. Z. Hatsagortsyan, B. J. Galow, and C. H. Keitel, Phys. Rev. Lett. **115**, 204801 (2015).

[55] X.-L. Zhu, Y. Yin, T.-P. Yu, F.-Q. Shao, Z.-Y. Ge, W.-Q. Wang, and J.-J. Liu, New J. Phys. **17**, 053039 (2015).

[56] D. J. Stark, T. Toncian, and A. V. Arefiev, Phys. Rev. Lett. **116**, 185003 (2016).

[57] K. V. Lezhnin, P. V. Sasorov, G. Korn, and S. V. Bulanov, Phys. Plasmas **25**, 123105 (2018).

[58] Y.-J. Gu, O. Klimo, S. V. Bulanov, and S. Weber, Commun. Phys. **1**, 93 (2018).

[59] T. W. Huang, C. M. Kim, C. T. Zhou, M. H. Cho, K. Nakajima, C. M. Ryu, S. C. Ruan, and C. H. Nam, New J. Phys. **21**, 013008 (2019).

[60] P. Hadjisolomou, T. M. Jeong, P. Valenta, D. Kolenaty, R. Versaci, V. Olšovcová, C. P. Ridgers, and S. V. Bulanov, J. Plasma Phys. **88**, 905880104 (2022).

[61] P. Hadjisolomou, T. M. Jeong, and S. V. Bulanov, Sci. Rep. **12**, 17143 (2022).

[62] P. Zhang, C. P. Ridgers, and A. G. R. Thomas, New J. Phys. **17**, 043051 (2015).

[63] T. Grismayer, M. Vranic, J. L. Martins, R. A. Fonseca, and L. O. Silva, Phys. Plasmas **23**, 056706 (2016).

[64] X.-L. Zhu, T.-P. Yu, Z.-M. Sheng, Y. Yin, I. C. E. Turcu, and A. Pukhov, Nat. Commun. **7**, 13686 (2016).

[65] M. Vranic, T. Grismayer, R. A. Fonseca, and L. O. Silva, Plasma Phys. Control. Fusion **59**, 014040 (2017).

[66] A. Gonoskov, A. Bashinov, S. Bastrakov, E. Efimenko, A. Ilderton, A. Kim, M. Marklund, I. Meyerov, A. Muraviev, and A. Sergeev, Phys. Rev. X **7**, 041003 (2017).

[67] Z. Gong, R. H. Hu, Y. R. Shou, B. Qiao, C. E. Chen, X. T. He, S. S. Bulanov, T. Z. Esirkepov, S. V. Bulanov, and X. Q. Yan, Phys. Rev. E **95**, 013210 (2017).

[68] E. S. Efimenko, A. V. Bashinov, S. I. Bastrakov, A. A. Gonoskov, A. A. Muraviev, I. B. Meyerov, A. V. Kim, and A. M. Sergeev, Sci. Rep. **8**, 2329 (2018).

[69] J. Vyskočil, O. Klimo, and S. Weber, Plasma Phys. Control. Fusion **60**, 054013 (2018).

[70] D. Kolenatý, P. Hadjisolomou, R. Versaci, T. M. Jeong, P. Valenta, V. Olšovcová, and S. V. Bulanov, Phys. Rev. Res. **4**, 023124 (2022).

[71] S. Chintalwad, S. Krishnamurthy, B. Ramakrishna, and C. P. Ridgers, Phys. Rev. E **105**, 025205 (2022).

[72] O. Budriga, L. E. Ionel, D. Tatomirescu, and K. A. Tanaka, Opt. Lett. **45**, 3454 (2020).

[73] J. Badziak, S. Jabłoński, T. Pisarczyk, P. Rączka, E. Krousky, R. Liska, M. Kucharik, T. Chodukowski, Z. Kalinowska, P. Parys *et al.*, Phys. Plasmas **19**, 053105 (2012).

[74] S. Busold, D. Schumacher, O. Deppert, C. Brabetz, S. Frydrych, F. Kroll, M. Joost, H. Al-Omari, A. Blažević, B. Zielbauer *et al.*, Phys. Rev. ST Accel. Beams **16**, 101302 (2013).

[75] I. Tsygvintsev, *Results of RHD simulation of ns-prepulse with 3DLINE code for different target materials* (Zenodo, 2022), https://doi.org/10.5281/zenodo.6412637.

[76] T. D. Arber, K. Bennett, C. S. Brady, A. Lawrence-Douglas, M. G. Ramsay, N. J. Sircombe, P. Gillies, R. G. Evans, H. Schmitz, A. R. Bell *et al.*, Plasma Phys. Control. Fusion **57**, 113001 (2015).

[77] A. V. Higuera and J. R. Cary, Phys. Plasmas **24**, 052104 (2017).

[78] C. Ridgers, J. Kirk, R. Duclous, T. Blackburn, C. Brady, K. Bennett, T. Arber, and A. Bell, J. Comput. Phys. **260**, 273 (2014).

[79] D. E. Spence, P. N. Kean, and W. Sibbett, Opt. Lett. **16**, 42 (1991).

[80] L. L. Ji, A. Pukhov, I. Y. Kostyukov, B. F. Shen, and K. Akli, Phys. Rev. Lett. **112**, 145003 (2014).

[81] M. J. Duff, R. Capdessus, D. D. Sorbo, C. P. Ridgers, M. King, and P. McKenna, Plasma Phys. Control. Fusion **60**, 064006 (2018).

[82] J. Vyskočil, E. Gelfer, and O. Klimo, Plasma Phys. Control. Fusion **62**, 064002 (2020).

[83] H. Bethe and W. Heitler, Proc. R. Soc. London Ser. A **146**, 83 (1934).

[84] J. Adam, L. Adamczyk, J. R. Adams, J. K. Adkins, G. Agakishiev, M. M. Aggarwal, Z. Ahammed, I. Alekseev, D. M. Anderson, A. Aparin *et al.* (STAR Collaboration), Phys. Rev. Lett. **127**, 052302 (2021).

[85] Y. He, T. G. Blackburn, T. Toncian, and A. V. Arefiev, Commun. Phys. **4**, 139 (2021).
[86] T. Heinzl, B. King, and A. J. MacLeod, Phys. Rev. A **102**, 063110 (2020).
[87] T. Heinzl and A. Ilderton, Opt. Commun. **282**, 1879 (2009).
[88] A. Di Piazza, Phys. Rev. Lett. **117**, 213201 (2016).
[89] D. Volkov, Z. Phys. **94**, 250 (1935).
[90] V. Baier, V. Katkov, and V. Strakhovenko, Nucl. Phys. B **328**, 387 (1989).
[91] V. Dinu, C. Harvey, A. Ilderton, M. Marklund, and G. Torgrimsson, Phys. Rev. Lett. **116**, 044801 (2016).
[92] A. Ilderton, B. King, and D. Seipt, Phys. Rev. A **99**, 042121 (2019).
[93] A. Di Piazza, M. Tamburini, S. Meuren, and C. H. Keitel, Phys. Rev. A **98**, 012134 (2018).
[94] B. King, Phys. Rev. A **101**, 042508 (2020).
[95] S. Meuren, K. Z. Hatsagortsyan, C. H. Keitel, and A. Di Piazza, Phys. Rev. D **91**, 013009 (2015).
[96] T. Podszus and A. Di Piazza, Phys. Rev. D **104**, 016014 (2021).
[97] M. Tamburini and S. Meuren, Phys. Rev. D **104**, L091903 (2021).
[98] T. Tajima and G. Mourou, Phys. Rev. ST Accel. Beams **5**, 031301 (2002).
[99] Z. Li, Y. Kato, and J. Kawanaka, Sci. Rep. **11**, 151 (2021).
[100] F. C. Salgado, K. Grafenstein, A. Golub, A. Döpp, A. Eckey, D. Hollatz, C. Müller, A. Seidel, D. Seipt, S. Karsch *et al.*, New J. Phys. **23**, 105002 (2021).
[101] J. van Tilborg, S. Steinke, C. G. R. Geddes, N. H. Matlis, B. H. Shaw, A. J. Gonsalves, J. V. Huijts, K. Nakamura, J. Daniels, C. B. Schroeder *et al.*, Phys. Rev. Lett. **115**, 184802 (2015).
[102] C. Ahdida, D. Bozzato, D. Calzolari, F. Cerutti, N. Charitonidis, A. Cimmino, A. Caronetti, G. L. D'Alessandro, A. Donadon Servelle, L. S. Esposito *et al.*, Front. Phys. **9**, 788253 (2022).
[103] J. Allison, K. Amako, J. Apostolakis, P. Arce, M. Asai, T. Aso, E. Bagli, A. Bagulya, S. Banerjee, G. Barrand *et al.*, Nucl. Instrum. Methods Phys. Res. Sect. A **835**, 186 (2016).